15TH IEA HEAT PUMP CONFERENCE
MAY 26–29, 2026 | HOFBURG
VIENNA 2026
DECARBONISATION THROUGH INNOVATION

Simulation and experimental validation of an integrated heat pump – thermal energy storage using a room-temperature phase change material

Al-Hussain Othman[a], James Tancabel[a], Vikrant Aute[a*], Yiyuan Qiao[b], Lingshi Wang[b], Zhenning Li[b], Yifeng Hu[b], Xiaobing Liu[b], Bo Shen[b], Kyle Gluesenkamp[b]

[a]Department of Mechanical Engineering, University of Maryland, College Park, MD 20742, United States
[b]Oak Ridge National Laboratory, 1 Bethel Valley Rd, Oak Ridge, TN 37830, United States

Abstract

As the dependence on electrical heat pumps (HPs) and intermittent renewables increases, grid strains are expected to grow. This necessitates an energy storage system to reduce the mismatch between energy supply and demand. Thus, a proposed dual-mode commercially available 14.1 kW HP was integrated with a single 22°C phase change material (PCM) thermal storage system (TES) to load-shift both cooling and heating loads. The HP-TES system was manufactured and experimentally tested using a novel test matrix based on AHRI 210/240 psychrometric conditions. Furthermore, transient dual-mode system-level HP-TES models were developed in Modelica and validated using the experimental test conditions. Base HP cooling and heating experimental tests at ambient temperatures of 35°C and −8.3°C show that the modified HP-TES maintained the rated system capacity and performance. The HP-TES discharge provided approximately 30% and 50% reductions in cooling and heating demand, respectively. The transient HP-TES models predicted system capacity and total power input for discharge and recharge operating modes within ±4% mean percentage error, and recharge power input within ±2%, with maximum errors occurring at the equipment startup. During system operation, the sources of model deviations are first-order polynomial fits of the PCM digital scanning calorimetry (DSC) data and unaccounted supercooling in the PCM during solidification. Nonetheless, the model predictions agree with the experimental tests, demonstrating the availability of robust, accurate, and validated transient models that can be used for further validation and the development of system controls.

Keywords: Heat pump; Thermal energy storage; phase-change material; Transient modeling; Experimental validations

1. Introduction

Commercial and residential buildings globally account for 30% of energy consumption, with space heating and cooling accounting for 45% and 20%, respectively [1], [2], [3]. In the United States, the EIA estimates that space conditioning (both heating and cooling) accounts for up to 50% of building energy use [4], with heat pumps outselling gas furnaces, increasing strain on the electrical grid [5]. With the growing reliance on intermittent renewable energy sources and dependence on heat pumps (HPs), grid strains are expected to increase. One possible solution is to integrate HPs with thermal energy storage (TES) technologies, specifically latent TES, to reduce the mismatch between energy supply and demand during peak hours [6], [7]. Latent TES was selected given its higher energy storage density per unit volume, and phase-change materials' (PCMs) lower costs [8], [9].

Integrated HP-TES systems have been widely investigated in the literature for their potential to reduce peak demand. Modeling approaches are usually quasi-steady-state, where the HPs are modeled either with system-efficiency maps [10], [11], [12] or steady-state models [13], [14] that are combined with transient models for the TES, e.g., detailed CFD models [15] or reduced-order capacitance-resistance approaches [16].

* Corresponding author. Tel.: +1-301-405-8726
E-mail address: vikrant@umd.edu

Experimental studies have been conducted to evaluate TES performance individually by Long & Zhu [17] and Shi et al. [18] for an underground TES coupled with a ground-source HP. Experimental studies of complete HP-TES systems conducted were application or mode-specific (cooling/heating), such as domestic hot-water TES [19], space-cooling-only TES [15], and space-heating-only HP-TES [20].

To the best of the authors' knowledge, the only work to validate a dual-mode HP-TES model was conducted by Hirschey et al. [13], who validated a steady-state model of the base HP and conducted parametric analyses of expected system performance for demand reduction and energy requirements. This work presented a more detailed model than the map-based HP models mentioned. Nonetheless, the dynamic nature of any HP-TES system requires accurate, validated system-level transient models. Therefore, in this study, a dual-mode single-room-temperature phase-change material (PCM) TES [21], aimed at reducing peak hour temperature lifts, was integrated with a commercially available rooftop unit (RTU) HP system and experimentally tested using a novel test matrix in cooling and heating modes [22]. Dual-mode system-level transient models were developed using an in-house Modelica library [23]. Model validations were conducted across a wide range of ambient conditions and HP-TES system operations, namely base HP (no TES), HP-TES discharge, and HP-TES recharge, including both continuous and cyclic operations to explore potential benefits from repeated transient operation. The findings demonstrate that the HP-TES system-level transient model accurately predicted experimental behavior for system base operation, discharge-demand reduction, and recharge performance.

2. Methodology

2.1. HP-TES Component and System Transient Models

The dual-mode HP-TES system was designed based on a commercially available 14.1 kW (4-ton) HP RTU [24]. The base RTU comprises two air-to-refrigerant louver-finned microchannel heat exchangers (MCHXs), a single-speed scroll compressor, and a thermostatic expansion valve (TXV). The thermal battery TES was sized to operate for at least 2 hours in cooling mode and integrated using a secondary hydronic loop using a brazed plate heat exchanger (BPHX) and a water pump. The TES was built with off-the-shelf finned-tube heat exchangers (FTHXs) submerged in a salt hydrate phase change material (PCM) with a 22°C nominal phase change temperature [21]. During HP-TES system integration, the TXV was removed and replaced with multiple electronic expansion valves (EXVs) to facilitate the implementation of HP-TES mode-specific controls [25]. The HP-TES has three operating modes for both heating and cooling operation: (a) base HP (Figure 1(a)); (b) the HP-TES discharge (Figure 1(b)); and (c) the HP-TES recharge (Figure 1(c)), for a total of six operating modes. Transient models of all HP-TES system operating modes were developed using an in-house Modelica library [23] that accounts for system dynamics during startup, operation, and shutdown.

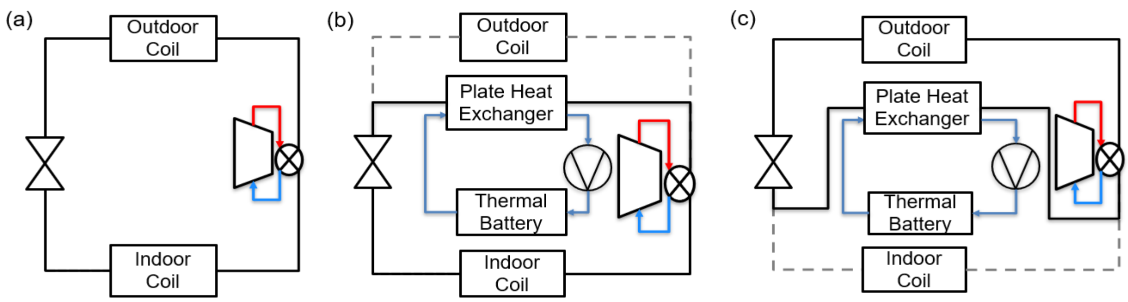

Figure 1. Model representations of (a) Base HP, (b) HP-TES discharge mode, and (c) HP-TES recharge mode

2.1.1. Heat Exchanger Models

In this HP-TES system, three types of heat exchangers (HXs) were utilized: air-to-refrigerant MCHXs, water-to-refrigerant BPHX, and PCM-to-water TES FTHXs. The Modelica-based HX models follow a segmented finite control volume (CV) approach for the refrigerant, water, and air, as shown in Figure 2. The heat transfer between CVs was connected using the Modelica Standard Library [26] specific HeatPorts. In all HX types, the tube wall thermal mass was considered, along with the corresponding wall thermal conductivity. For all finned surfaces, the wall CV lumps both the wall and fin thermal masses and equivalent thermal conductivities.

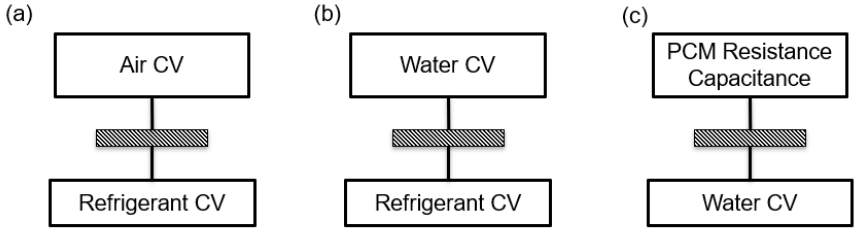

Figure 2. Modelica model representations for (a) air-to-refrigerant microchannel heat exchangers, (b) water-to-refrigerant brazed plate heat exchangers, and (c) PCM-to-water TES heat exchangers

The air- or water-to-refrigerant HXs (MCHX and BPHX) were modeled considering the side transient mass (Eq.(1)) and energy balances (Eq.(2)) [23], [27], [28] in its corresponding refrigerant CV. The state variables were the Pressure (P) and Enthalpy (h). In both HXs, the heat transfer was assumed to be one-dimensional, neglecting axial conduction and refrigerant maldistribution. The heat transfer coefficient (α) correlations for all HXs are summarized in Table 1.

$$\frac{dM}{dt} = V\frac{D\rho}{Dt} = \dot{m}_{in} - \dot{m}_{out} \tag{1}$$

$$\frac{dE}{dt} = V\frac{D}{Dt}\left(\rho h - P\right) = \dot{m}_{in}h_{in} - \dot{m}_{out}h_{out} + \alpha_{ref}A(T_{ref} - T_{wall}) \tag{2}$$

Table 1. Single and two-phase heat transfer correlations that are utilized in all HX models

HX	Single-Phase HTC	Two-phase HTC
MCHX Condensing	Gnielinski [29]	Shah [30]
MCHX Evaporating	Gnielinski [29]	Shah [31]
BPHX Condensing	Muley & Manglik [32]	Yan et al. [33]
BPHX Evaporating	Muley & Manglik [32]	Jo et al. [34]
PCM-TES	Dittus & Boelter [35]	N/A

For the air-to-refrigerant MCHX, the air-side CV assumes quasi-steady-state mass and energy balances, as mentioned in Qiao et al. [23]. Furthermore, the heat transfer between the air and the wall CVs is assumed to be one-dimensional, with uniform airflow across all MCHX tubes. Fin efficiency was accounted for in the sensible heat transfer calculation Eq.(3), as the wall CV surface temperature is assumed to be uniform across the tube and fins. The air-side heat transfer coefficient (α) was obtained from the louver-finned Chang & Wang [36] correlation.

$$\dot{Q}_{sens} = \alpha(A_p + \eta_{fin}A_s)(T_{wall} - T_{air,in}) \tag{3}$$

The total (sensible and latent) air-side heat transfer is shown in Eq.(4) using the inlet and outlet temperatures and humidity ratios. For latent heat transfer, the condensate enthalpy of vaporization $(h_{fg,water})$ was computed at the wall surface temperature. The outlet humidity ratio was calculated using the Lewis analogy [37], where $Le^{2/3} = 0.9$ [38], as shown in Eq.(5). Given flow uniformity assumptions on the refrigerant and air side, the condensate formation was similarly uniform. More details on the refrigerant and air-side control volumes can be found in Qiao et al. [23] and Dhumane et al. [27].

$$\dot{Q}_{tot,air} = \dot{m}_{air}\left[C_{p,a}(T_{in,air} - T_{out,air}) + h_{fg,water}(\omega_{in,air} - \omega_{out,air})\right] \tag{4}$$

$$\omega_{out,air} = \omega_{in,air} + \min(0, \omega_{wall,sat} - \omega_{in,air})\left(1 - \exp\left(\frac{-\alpha(A_p + \eta_{fin}A_s)}{\dot{m}_{air}c_{p,air}Le^{2/3}}\right)\right) \tag{5}$$

For the secondary hydronic loop HXs, i.e., the BPHX (Figure 2(b)) and PCM-HXs (Figure 2(c)), the water CV was utilized, which employs the transient mass and energy balance equations (Eq.(6)), with the water-side heat transfer coefficients determined using the correlation in Table 1. On the PCM side, a resistance-capacitance approach was used [16], [27], [39]. The resistance term accounts for conduction-only heat transfer between the PCM and the HX tube walls, using the PCM's thermal conductivity. The capacitance refers to the time-dependent energy stored or released in the PCM, referring to the transient PCM thermal mass term in Eq.(7). The change in PCM energy storage during melting and solidification was determined from the change in PCM storage enthalpy over time, based on manufacturer-provided digital scanning calorimetry (DSC) curves [40]. Additionally, a convective heat-loss term was included to account for natural convection heat losses to the ambient. The heat transfer was assumed to be 1-D, and PCM stratification during off-periods and cyclic operations was neglected.

$$\rho_i V_i C_{p,i} \frac{dT_i}{dt} = \alpha_i A_i (T_{wall,i} - T_{water,i-1}) + \dot{m}_i h_i - \dot{m}_{i+1} h_{i+1} \tag{6}$$

$$\frac{dh_{PCM,i}}{dt} M_{PCM,i} = \frac{k}{L} A_j (T_{wall,i} - T_{water,i-1}) + \dot{Q}_{loss} \tag{7}$$

2.1.2. Compressor, Expansion Device, and Water Pump

The single-speed scroll compressor was modeled using the manufacturer-specified AHRI 210/240 [41] 10-coefficient compressor maps with Dabiri & Rice [42] suction superheat correction. Convective heat loss through the compressor shell was also considered [23]. The PI-EXV is treated as a variable-orifice model, adjusting the valve opening (Eq.(8)) to match a setpoint parameter, i.e., compressor suction superheat or condenser outlet subcooling, chosen based on the experimental control parameter.

$$\dot{m}_{EXV} = \frac{u}{u_{max}} C_v A \sqrt{\rho_{in} \Delta P} \tag{8}$$

The water pump power was calculated from experimentally-determined pump efficiencies, secondary loop pressure drops, and measured water flow rate using Eq.(9). The steady-state pump model accounts for water heat gain from the pump motor (Eq.(10)).

$$\dot{W}_{pump} = \frac{\dot{m}_{water} (\Delta P)}{\eta_{pump} \rho_{in}} \tag{9}$$

$$\dot{Q}_{gain} + \dot{m}_{water} h_{in} - \dot{m}_{water} h_{out} = 0 \tag{10}$$

2.2. HP-TES Experimental Setup

The 14.1 kW dual-mode HP-TES system was prototyped using a commercially available RTU and integrated with a PCM-HX using a 22°C PCM via a secondary hydronic loop containing a brazed plate heat exchanger (BPHX) and a single-speed water pump. The HP-TES was instrumented and tested in the psychrometric chambers at the Oak Ridge National Laboratory (Figure 3) [43]. The instruments utilized and their uncertainties are displayed in Table 2. The modified RTU HP-TES was equipped with several EXVs used for mode-specific controls. The operating modes include base HP, HP-TES discharge, and recharge in both cooling and heating operations. For each mode, specific control targets were set to ensure reliable operation and smooth mode transitions. More information on the system experimental setup and controls can be found at Qiao et al. [25].

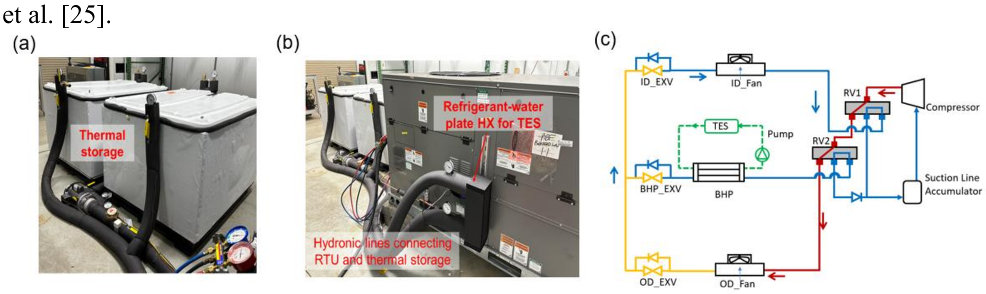

Figure 3. HP-TES system in the experimental facility at ORNL: (a) PCM- HX TES; (b) complete integrated system connected RTU HP-TES connected through BPHX; (c) the experimental schematic [43], [25]

Table 2. HP-TES Instrumentation and uncertainties [44]

Measured Parameter	Instrument	Range	Uncertainty
Refrigerant temperature (T_{ref})	T-type thermocouples	−270 – 370°C	±0.5°C
Refrigerant pressure (P_{ref})	Omega PX409 transducers	0 – 5.2 MPa	±0.08% BSL maximum
Water flow rate ($\dot{V}_{water}$)	Vortex shedding flow meter FV103	0.57 – 5.7 m^3/h	±2% of reading
Water temperature (T_{water})	SA 1 RTD	−73 – 260°C	±0.15°C
Air flow rate ($\dot{V}_{air}$)	Foxboro differential pressure transducer IDP10S	1.2 – 500 mbar	±0.05% of reading
Air temperatures (T_{db} / T_{wb})	Rosemount Platinum RTD PT100	−1.95 – 600°C	±0.15°C
Total power ($\dot{W}_{total}$)	Yokogawa GE WT333e power meter	15 – 600 V; 0.5 – 20 A	±(0.1% of reading +0.05% of range)

2.3. HP-TES Experimental Test Matrix

A novel laboratory test matrix, based on the AHRI Standard 210/240 [45], was developed and tested, comprising 22 tests (11 in cooling mode, and 11 in heating mode) [22]. Experimental validations were conducted for six of these cases: three cooling (Table 3) and three heating (Table 4), including baseline HP and continuous HP-TES system discharge and recharge operating modes at multiple ambient temperature conditions. The tested conditions were conducted to ensure consistent base HP operation with manufacturer data, evaluate HP-TES performance and the potential for demand reduction, and identify suitable conditions for TES recharge.

Table 3. HP-TES cooling mode test matrix [22]

Test	Cooling Test Type	Outdoor T_{db} / T_{wb} (°C)	Indoor T_{db} / T_{wb} (°C)
1C	Conventional (Base HP-only), unfavorable ambient	35.0 / 23.9 (A_{Full})	26.7 / 19.4
3C	Continuous discharge: SOC 1→0, unfavorable ambient	35.0 / 23.9 (A_{Full})	26.7 / 19.4
9C	Continuous recharge: SOC 0→1, semi-favorable ambient	27.8 / 18.3 (B_{Full})	26.7 / 19.4

Table 4. HP-TES heating mode test matrix[22]

Test	Heating Test Type	Outdoor T_{db} / T_{wb} (°C)	Indoor T_{db} / T_{wb} (°C)
6H	Conventional (Base HP-only), unfavorable ambient	−8.3 / −9.4 ($H3_{Full}$)	21.1 / 15.6
8H	Continuous discharge: SOC 1→0, unfavorable ambient	−8.3 / −9.4 ($H3_{Full}$)	21.1 / 15.6
10H	Continuous recharge: SOC 0→1, unfavorable ambient	−15.0 / −16.1 ($H4_{Full}$)	21.1 / 15.6

3. Results and Discussion

3.1. Base HP Mode Model Validation

Base HP cooling (1C: T_{db} / T_{wb} = 35.0°C / 23.9°C) and heating (6H: T_{db} / T_{wb} = −8.3°C / −9.4°C) tests were conducted to ensure the modified HP-TES system performance is consistent with the manufacturer's data. In cooling mode (Figure 4(a)), the unit showed no capacity degradation, maintaining a cooling capacity of 14.0 ± 0.69 kW and a total power of 4.0 ± 0.01 kW, aligning with the manufacturer's catalog data: 13.8 kW capacity and a total power consumption of 3.8 kW [24]. In heating mode (Figure 4(b)), a 15% capacity degradation was observed, corresponding to a heating capacity of 7.9 ± 0.69 kW, which was expected to result from heat loss through the RTU cabinet. The modified HP-TES unit provided a slightly higher system capacity than the manufacturer’s data under similar conditions. This can be seen in the catalog, where the heating capacities ranged between 6.8 kW and 7.8 kW for ambient conditions of −9.4°C and −6.7°C, respectively [24].

In both cooling and heating modes, the HP-TES model accurately predicts overall system performance within 1% for both capacity and power, thus well within the experimental uncertainty. The only deviations occurred during system start-up, as expected, since the reported experimental data were steady-state, while the Modelica model assumes a system start-up period. However, the steady-state model performance matches very well, thus validating the model predictions.

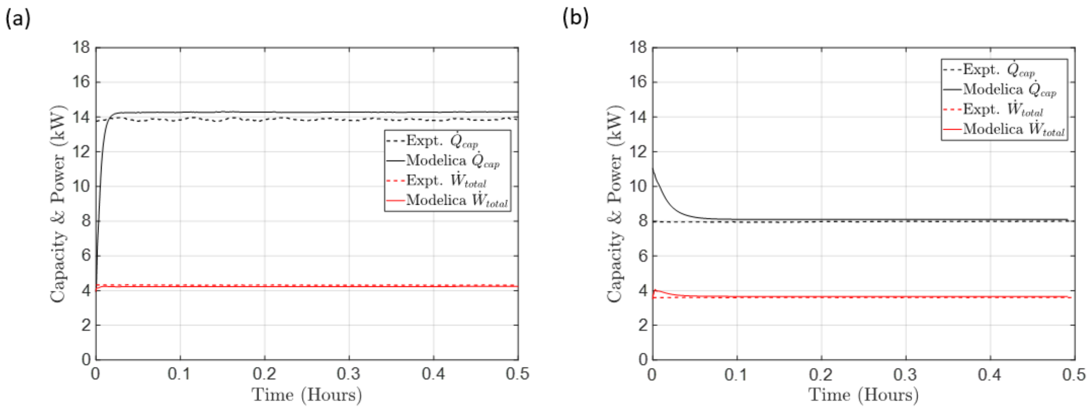

Figure 4. Base HP model validations in (a) cooling mode (test 1C: 35.0 / 23.9 °C) and (b) heating mode (test 6H: −8.3°C / −9.4°C)

3.2. HP-TES Cooling Mode Model Validation

Discharge test 3C was conducted under AHRI 210/240 A-test ambient conditions [45], and therefore compared with the base HP Test 1C (Figure 4(a)). This was an ideal test to demonstrate the HP-TES system's capability in isolating the vapor-compression in warm US climate zones (e.g., Florida, Arizona, California) using TMY3 data [46]. Experimentally, the discharge test showed that the HP-TES exceeded the rated AHRI Standard 210/240 [45] A-Test 14.0 kW capacity by 7% at the beginning and overlapped at the end of the 2-hour test period, with lower compressor power (Figure 5). This occurred because the compressor temperature and pressure lifts reduced, due to the room-temperature PCM lowering the compressor discharge conditions. The experimental demand reduction when using the HP-TES versus the base HP mode was 31.2%. HP-TES model validations demonstrate excellent agreement in cooling capacity, system input power, and compressor inlet and outlet pressures throughout the TES discharge process, with slight deviations. These deviations were primarily due to the water temperatures entering and leaving the TES systems, with a 3K difference. Possible reasons for these differences include heat gains through the hydronic loop piping and components, especially at 35°C. Nonetheless, the overall system-level predictions were acceptable, with the maximum cooling capacity error less than 4%.

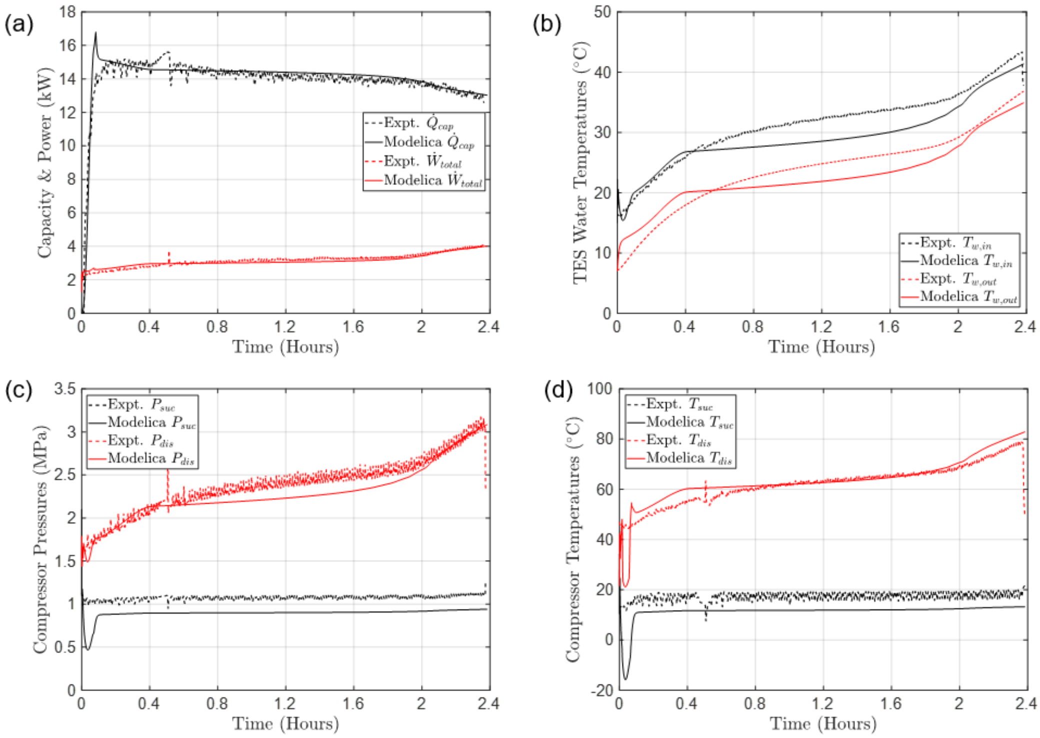

Figure 5. Model validations for test 3C (35.0 / 23.9 °C): (a) capacity & power, (b) TES inlet & outlet temperatures, compressor suction/discharge (c) pressure, and (d) temperature

Recharge test 9C occurs at semi-favorable AHRI 210/240 B-Test conditions (27.8°C / 18.3°C) [45], given the lower temperature difference between the heat source and the sink (PCM temperature). For recharge mode, the HP-TES system uses the outdoor MCHX as the condenser and the BPHX (and thus TES) as the evaporator to solidify the PCM for the next day's use. Overall, the HP-TES model accurately predicts HP-TES performance (Figure 6), compressor temperatures, and TES water temperatures, even in the presence of PCM supercooling. The deviation in the TES water temperatures was due to the DSC curves not representing any supercooling data [47]. The deviations at the start-up and end points occur due to a high degree of oscillatory superheat during the experiment, whereas the model used constant superheat setpoints.

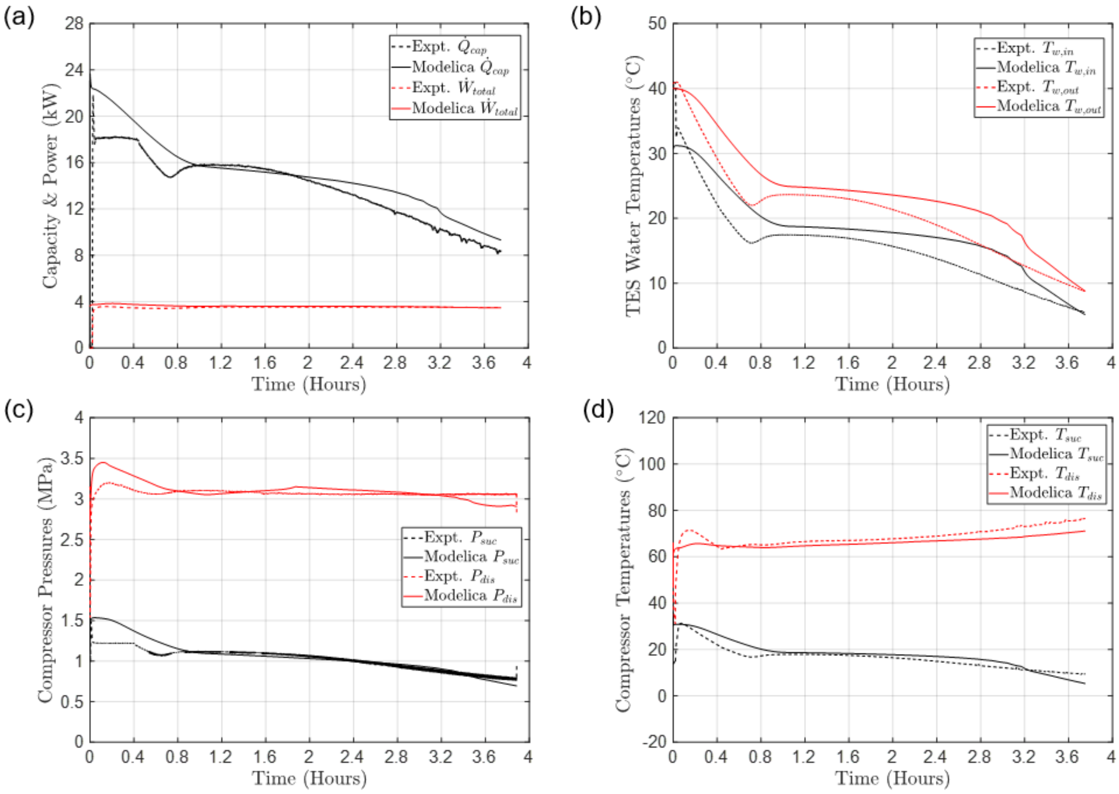

Figure 6. Model validations for test 9C (27.8°C/18.3°C): (a) capacity & power, (b) TES inlet & outlet temperatures, compressor suction/discharge (c) pressure, and (d) temperature

3.3. HP-TES Heating Mode Model Validation

Similarly, HP-TES heating mode validations were conducted for two tests: discharge and recharge. Discharge test 8H was conducted under considerably cold conditions, corresponding to the AHRI 210/240 H3 Test conditions (−8.3°C/−9.4°C) [45]. These conditions resulted in a 15% capacity degradation when the base HP was operating, prompting the need for backup heating. The discharge test showed that the HP-TES discharge heating capacity exceeded the 14.1 kW nominal rating by 20% at the start and remained above that level for 2.6 hours, with the compressor requiring 50.8% less electrical power. This indicates that the TES successfully isolated the HP system from outdoor conditions, increasing the compressor suction temperature and pressure. A key outcome of this integrated HP-TES system is the elimination of backup heating during peak hours, further reducing grid strain and/or reliance on natural gas in cold-climate regions. Model validations conducted demonstrated a good agreement in heating capacity, system input power, TES inlet and outlet conditions, and compressor inlet and outlet refrigerant pressures and temperatures throughout the discharge process, with only slight deviations. The deviations occurred primarily due to slight PCM supercooling 30 minutes into the test and discontinuities that happened during the test, caused by refrigerant escaping to unused cycle components (i.e., the outdoor coil). Therefore, the next steps will include improving the DSC curve-fits. Nonetheless, the capacity and power requirements are within the experimental uncertainties, indicating good performance predictions.

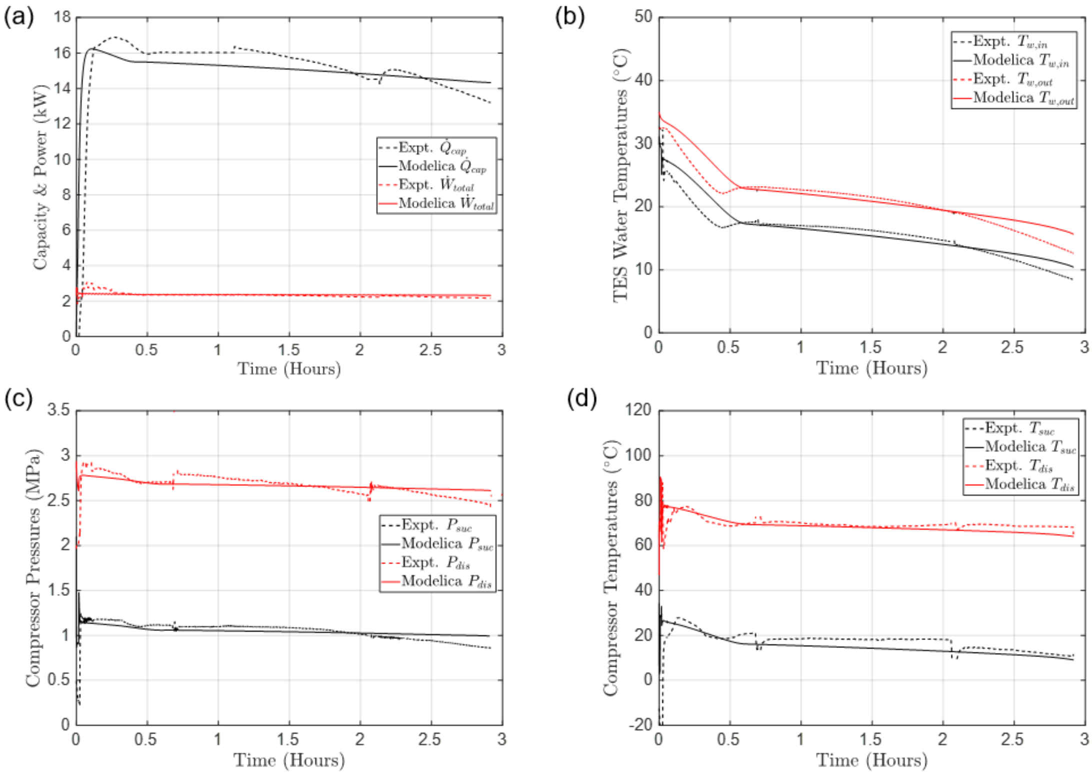

Figure 7. Model validations for test 8H (-8.3°C/-9.4°C): (a) capacity & power, (b) TES inlet & outlet temperatures, compressor suction/discharge (c) pressure, and (d) temperature

HP-TES continuous recharge model validation in heating mode unit was conducted on test case 10H, which corresponds to the AHRI H4 test condition of $T_{db} / T_{wb} = -15.0°C / -16.1°C$. This test was conducted under extreme cold-climate conditions to evaluate HP-TES recharge performance. This test case results show that the overall recharge capacity degraded to 60% of the RTU's base nominal capacity. This occurred as the compressor suction pressures and temperatures decreased significantly, resulting in lower refrigerant densities and, consequently, reducing refrigerant mass flow rates and recharge capacities. Moreover, the impact of heat loss from the TES to the surroundings was pronounced under these conditions, almost doubling the time required to recharge the TES compared with discharge periods, and resulting in an incomplete recharge. Model validations conducted for test 10H show good agreement between experimental recharge capacities, power requirements, and compressor suction and discharge temperatures and pressures (Figure 8). Nonetheless, deviations in discharge temperatures are higher at the beginning of the test. These deviations can be attributed to significant heat loss through the compressor shell and to lower initial system temperatures before testing. However, as the system heated up, both discharge pressures and temperatures agreed. This test is a clear indicator of the necessity to locate the most rechargeable ambient conditions, primarily by reducing the recharge temperature lift and minimizing off-peak energy requirements, rather than creating a nocturnal artificial peak [48].

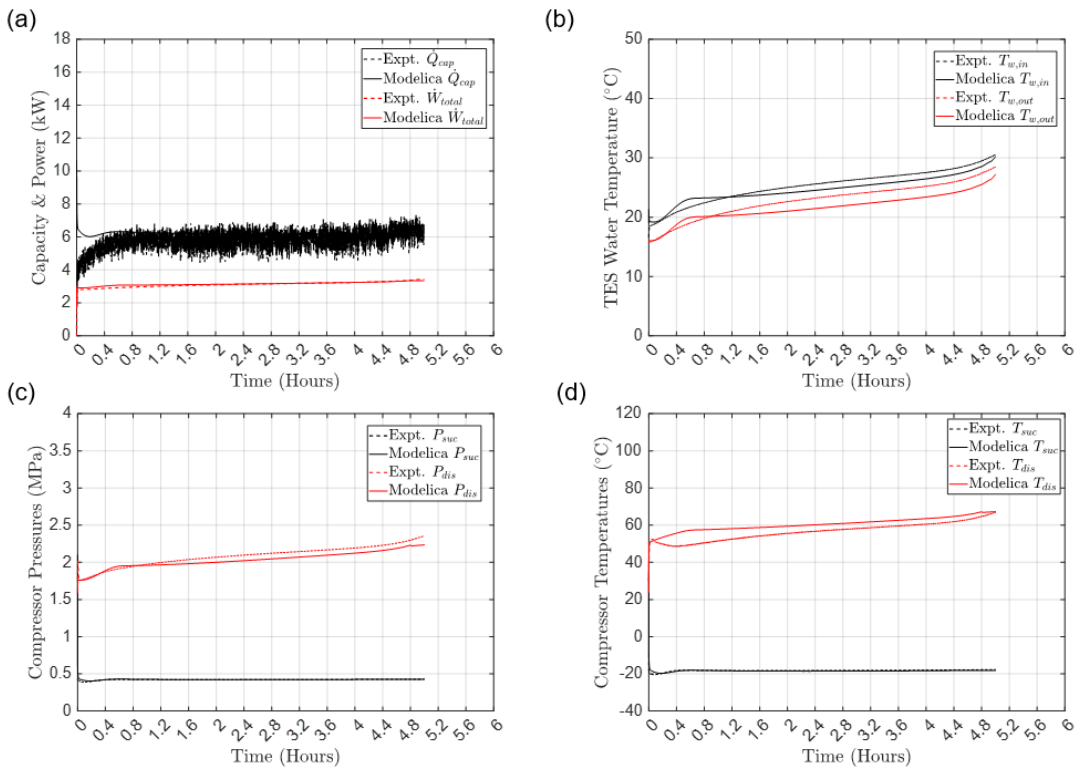

Figure 8. Model validations for test 10H (-15.0°C/-16.1°C): (a) capacity & power, (b) TES inlet & outlet temperatures, compressor suction/discharge (c) pressure, and (d) temperature

4. Conclusions

In this work, a dual-mode 14.1 kW R410A HP-TES unit was prototyped using an RTU HP integrated with a single-room-temperature PCM-HX via a secondary hydronic loop and experimentally tested under controlled psychrometric conditions based on AHRI Standard 210/240 [23]. Transient models of the HP-TES system were developed using an in-house Modelica library and validated across a wide range of tests under different operating ambient conditions and modes (i.e., base HP mode, continuous discharge, and continuous recharge). Base HP experimental tests indicated that the modified RTU HP-TES unit performance remained consistent with the manufacturer's catalog data, ensuring no capacity degradation, and the base HP model validations showed an excellent agreement of less than 1% in system capacity and power demand at steady-state conditions. Experimental HP-TES discharge demonstrated a 30% demand reduction in cooling mode at AHRI 210/240 A-Test conditions, and 51% in heating mode operating at AHRI 210/240 H3-Test conditions. Potentially higher peak reductions in heating mode can be achieved when considering that the HP-TES system eliminates the need for backup heating. Not considering system startup, the transient HP-TES models predicted system capacity and total power input for discharge and recharge operating modes within ±4% mean percentage deviation, and recharge power input within ±2%. The maximum deviations occur at startup due to rapid changes in system-level control and the unknown initial states of components. Current model limitations were primarily due to heat losses or gains through the hydronic loop components and to the unaccounted supercooling in the PCM during solidification, which will be addressed in the next steps. Despite these differences, the overall excellent validations instilled confidence in the developed models and demonstrated the load-shifting value of integrated HP-TES systems.

5. Nomenclature

Abbreviations		L	Tube spacing [m]
BPHX	Brazed plate heat exchanger	M	Mass [kg]
COP	Coefficient of performance	$\dot{m}$	Mass flow rate [kg s^{-1}]
CV	Control volume	P	Pressure [Pa]
DB	Dry-bulb	ΔP	Pressure drop [Pa]
EXV	Electronic expansion valve	$\dot{Q}$	Heat transfer rate [kW]

HP	Heat pump	T	Temperature [K]
MCHX	Microchannel heat exchanger	t	Time [s]
PCM	Phase change material	u / u_{max}	EXV step opening [-]
TES	Thermal energy storage	$\dot{W}_{total}$	Total power [kW]
Symbols		U	Uncertainty
A	Area [m^2]	***Greek Letters***	
C_v	Expansion valve coefficient [-]	α	Heat transfer coefficient [$Wm^{-2}K^{-1}$]
H_{sl}	Enthalpy of fusion [kJ kg^{-1}]	η_{fin}	Fin efficiency [-]
h	Enthalpy [kJ kg^{-1}]	ρ	Density [kg m^{-3}]
k	Thermal Conductivity [$Wm^{-1}K^{-1}$]	ω	Humidity ratio [$kg_w\ kg_{da}^{-1}$]

Acknowledgements

This material is based upon work supported by the U.S. Department of Energy's Office of Energy Efficiency and Renewable Energy (EERE) under the Building Technologies Office (BTO) Award Number DE-EE0009681. The views expressed herein do not necessarily represent the views of the U.S. Department of Energy or the United States Government. This work was also supported in part by the Modeling & Optimization Consortium (MOC) at the Center for Environmental Energy Engineering (CEEE) at the University of Maryland.

The authors would also like to acknowledge additional collaborators from the Oak Ridge National Laboratory (Tim Dyer, Troy Seay, James Manley, Josh Standifer, Charlie Pierce, Mike Day), Electric Power Research Institute (A. Amarnath, G. Bailey, S. Goedeke, E. Hornquist, M. Robinson, M. Sweeney), Rheem Manufacturing Company (W. Elliott, H. Inamdar), Heat Transfer Technologies, LLC (J. Black, N. Carmeli-Shabtay, Y. Shabtay), and Insolcorp, LLC (M. Dunn, P. Horwath, J. Lippin) whose expertise contributed to the design, fabrication, system integration, experimental test matrix development, and evaluation of the prototype HP-TES unit.

References

[1] IEA, "Is cooling the future of heating? – Analysis," IEA. Accessed: Feb. 13, 2024. [Online]. Available: https://www.iea.org/commentaries/is-cooling-the-future-of-heating

[2] IEA, "The Future of Cooling –Opportunities for energy-efficient air conditioning," International Energy Agency (IEA), 2018. Accessed: Jun. 10, 2022. [Online]. Available: https://www.iea.org/reports/the-future-of-cooling

[3] IEA, "Cooling," IEA. Accessed: Feb. 09, 2024. [Online]. Available: https://www.iea.org/energy-system/buildings/space-cooling

[4] "U.S. EIA." Accessed: Dec. 23, 2024. [Online]. Available: https://www.eia.gov/todayinenergy/detail.php?id=61903

[5] "Monthly Shipments | AHRI." Accessed: Jul. 13, 2025. [Online]. Available: https://www.ahrinet.org/analytics/statistics/monthly-shipments

[6] H. A. Behabtu *et al.*, "A Review of Energy Storage Technologies' Application Potentials in Renewable Energy Sources Grid Integration," *Sustainability*, vol. 12, no. 24, p. 10511, Jan. 2020, doi: 10.3390/su122410511.

[7] Z. Chen, X. Zhang, J. Ji, and Y. Lv, "A review of the application of hydrated salt phase change materials in building temperature control," *J. Energy Storage*, vol. 56, p. 106157, Dec. 2022, doi: 10.1016/j.est.2022.106157.

[8] J. Hirschey, N. Kumar, T. Turnaoglu, K. Gluesenkamp, and S. Graham, "Review of Low-Cost Organic and Inorganic Phase Change Materials with Phase Change Temperature between 0°C and 65°C," *Int. High Perform. Build. Conf.*, May 2021, [Online]. Available: https://docs.lib.purdue.edu/ihpbc/389

[9] S. Mondal, "Phase change materials for smart textiles – An overview," *Appl. Therm. Eng.*, vol. 28, no. 11, pp. 1536–1550, Aug. 2008, doi: 10.1016/j.applthermaleng.2007.08.009.

[10] A. Arteconi, N. J. Hewitt, and F. Polonara, "Domestic demand-side management (DSM): Role of heat pumps and thermal energy storage (TES) systems," *Appl. Therm. Eng.*, vol. 51, no. 1, pp. 155–165, Mar. 2013, doi: 10.1016/j.applthermaleng.2012.09.023.

[11] F. Bruno, N. H. S. Tay, and M. Belusko, "Minimising energy usage for domestic cooling with off-peak PCM storage," *Energy Build.*, vol. 76, pp. 347–353, Jun. 2014, doi: 10.1016/j.enbuild.2014.02.069.

[12] R. Hirmiz, H. M. Teamah, M. F. Lightstone, and J. S. Cotton, "Performance of heat pump integrated phase change material thermal storage for electric load shifting in building demand side management," *Energy Build.*, vol. 190, pp. 103–118, May 2019, doi: 10.1016/j.enbuild.2019.02.026.

[13] J. Hirschey, Z. Li, K. R. Gluesenkamp, T. J. LaClair, and S. Graham, "Demand reduction and energy saving potential of thermal energy storage integrated heat pumps," *Int. J. Refrig.*, vol. 148, pp. 179–192, Apr. 2023, doi: 10.1016/j.ijrefrig.2023.01.026.

[14] C. Ermel, M. V. A. Bianchi, and P. S. Schneider, "Energy Model to Evaluate Thermal Energy Storage Integrated with Air Source Heat Pumps: Preprint," *Renew. Energy*, 2023.

[15] H. Zheng, C. Wang, Q. Liu, Z. Tian, and X. Fan, "Thermal performance of copper foam/paraffin composite phase change material," *Energy Convers. Manag.*, vol. 157, pp. 372–381, Feb. 2018, doi: 10.1016/j.enconman.2017.12.023.

[16] M. Menezes, J. Tancabel, D. Bacellar, and V. Aute, "Development & Experimental Validation of a Generalized Resistance-Capacitance Model for Numerical Simulation of Phase-Change Material Embedded Heat Exchangers," *Int. Refrig. Air Cond. Conf.*, Jan. 2024, [Online]. Available: https://docs.lib.purdue.edu/iracc/2568

[17] J.-Y. Long and D.-S. Zhu, "Numerical and experimental study on heat pump water heater with PCM for thermal storage," *Energy Build.*, vol. 40, no. 4, pp. 666–672, Jan. 2008, doi: 10.1016/j.enbuild.2007.05.001.

[18] L. Shi, M. Qu, X. Liu, L. Wang, and M. Zhang, "Numerical modeling and parametric study of a dual purpose underground thermal battery," *Energy Build.*, vol. 275, p. 112472, Nov. 2022, doi: 10.1016/j.enbuild.2022.112472.

[19] A. Frazzica, M. Manzan, A. Sapienza, A. Freni, G. Toniato, and G. Restuccia, "Experimental testing of a hybrid sensible-latent heat storage system for domestic hot water applications," *Appl. Energy*, vol. 183, pp. 1157–1167, Dec. 2016, doi: 10.1016/j.apenergy.2016.09.076.

[20] Ç. Yıldız, M. Seçilmiş, M. Arıcı, M. S. Mert, S. Nižetić, and H. Karabay, "An experimental study on a solar-assisted heat pump incorporated with PCM based thermal energy storage unit," *Energy*, vol. 278, p. 128035, Sep. 2023, doi: 10.1016/j.energy.2023.128035.

[21] "Solutions," Insolcorp, LLC. Accessed: Jan. 10, 2025. [Online]. Available: https://insolcorp.com/products/

[22] J. Tancabel *et al.*, "Performance Assessment of a Heat Pump Integrated with Thermal Energy Storage in Cooling & Heating Modes," presented at the ASHRAE Winter Conference 2025, [Unpublished manuscript].

[23] H. Qiao, V. Aute, and R. Radermacher, "Transient modeling of a flash tank vapor injection heat pump system – Part I: Model development," *Int. J. Refrig.*, vol. 49, pp. 169–182, Jan. 2015, doi: 10.1016/j.ijrefrig.2014.06.019.

[24] "Renaissance Commercial HVAC Line | Packaged G/E, A/C, and Heat Pumps | Rheem Commercial Air," Rheem. Accessed: Oct. 29, 2025. [Online]. Available: https://discover.rheem.com/commercial-air/renaissance-packaged

[25] Y. Qiao *et al.*, "Experimental study of a thermal energy storage-integrated heat pump system for load shifting in space cooling and heating," *Appl. Therm. Eng.*, vol. 290, p. 129992, Apr. 2026, doi: 10.1016/j.applthermaleng.2026.129992.

[26] *Modelica Standard Library*. (Mar. 22, 2024). Modelica. Modelica Association. Accessed: Mar. 22, 2024. [Online]. Available: https://github.com/modelica/ModelicaStandardLibrary

[27] R. Dhumane *et al.*, "Enhancing the thermosiphon-driven discharge of a latent heat thermal storage system used in a personal cooling device," *Int. J. Refrig.*, vol. 88, pp. 599–613, Apr. 2018, doi: 10.1016/j.ijrefrig.2018.02.005.

[28] R. Dhumane *et al.*, "Improving system performance of a personal conditioning system integrated with thermal storage," *Appl. Therm. Eng.*, vol. 147, pp. 40–51, Jan. 2019, doi: 10.1016/j.applthermaleng.2018.10.004.

[29] V. Gnielinski, "On heat transfer in tubes," *Int. J. Heat Mass Transf.*, vol. 63, pp. 134–140, 2013, doi: https://doi.org/10.1016/j.ijheatmasstransfer.2013.04.015.

[30] M. M. Shah, "Improved correlation for heat transfer during condensation in conventional and mini/micro channels," *Int. J. Refrig.*, vol. 98, pp. 222–237, Feb. 2019, doi: 10.1016/j.ijrefrig.2018.07.037.

[31] M. M. Shah, "Unified correlation for heat transfer during boiling in plain mini/micro and conventional channels," *Int. J. Refrig.*, vol. 74, pp. 606–626, Feb. 2017, doi: 10.1016/j.ijrefrig.2016.11.023.

[32] A. Muley and R. M. Manglik, "Experimental Study of Turbulent Flow Heat Transfer and Pressure Drop in a Plate Heat Exchanger With Chevron Plates," *J. Heat Transf.*, vol. 121, no. 1, pp. 110–117, Feb. 1999, doi: 10.1115/1.2825923.

[33] Y.-Y. Yan, H.-C. Lio, and T.-F. Lin, "Condensation heat transfer and pressure drop of refrigerant R-

134a in a plate heat exchanger," *Int. J. Heat Mass Transf.*, vol. 42, no. 6, pp. 993–1006, Mar. 1999, doi: 10.1016/S0017-9310(98)00217-8.

[34] C. Jo, D. Lee, H. J. Chung, Y. Kang, and Y. Kim, "Comparative evaluation of the evaporation heat transfer characteristics of a low-GWP refrigerant R-1234ze(E) between shell-and-plate and plate heat exchangers," *Int. J. Heat Mass Transf.*, vol. 153, p. 119598, Jun. 2020, doi: 10.1016/j.ijheatmasstransfer.2020.119598.

[35] F. W. Dittus and L. M. K. Boelter, "Heat transfer in automobile radiators of the tubular type," *Univ. Calif. Publ. Eng.*, vol. 12, no. 1, pp. 3–22, Oct. 1930, doi: 10.1016/0735-1933(85)90003-X.

[36] Y.-J. Chang and C.-C. Wang, "A generalized heat transfer correlation for Iouver fin geometry," *Int. J. Heat Mass Transf.*, vol. 40, no. 3, pp. 533–544, Feb. 1997, doi: 10.1016/0017-9310(96)00116-0.

[37] K. T. Hong and R. L. Webb, "Calculation of Fin Efficiency for Wet and Dry Fins," *HVACR Res.*, vol. 2, no. 1, pp. 27–41, Jan. 1996, doi: 10.1080/10789669.1996.10391331.

[38] T. H. (Thomas H.) Kuehn, "Thermal environmental engineering," *No Title*, Accessed: Apr. 09, 2024. [Online]. Available: https://cir.nii.ac.jp/crid/1130282270644812672

[39] T. Alam, G. Righetti, D. Bacellar, V. Aute, and S. Mancin, "Development and Validation Of Resistance-Capacitance Model (RCM) For Phase Change Material (PCM) Embedded In 3D Periodic Structures," *Int. Refrig. Air Cond. Conf.*, Jul. 2022, [Online]. Available: https://docs.lib.purdue.edu/iracc/2300

[40] M. Dunn, "Private communications," Mar. 23, 2023.

[41] AHRI Standard 540, "AHRI 540 (SI/ I-P): Performance Rating of Positive Displacement Refrigerant Compressors and Compressor Units | AHRI," 2020.

[42] A. E. Dabiri and C. K. Rice, "Compressor-simulation model with corrections for the level of suction gas superheat," Oak Ridge National Lab., TN (USA); Science Applications, Inc., La Jolla, CA (USA), CONF-810657-2, Jan. 1981. Accessed: Apr. 10, 2023. [Online]. Available: https://www.osti.gov/biblio/6345140

[43] K. R. Gluesenkamp, B. Shen, and Z. Li, "Packaged Multi-Functional Air Source Heat Pump Integrated with a Hydronic Loop for Cooling/Heating Energy Storage," Aug. 22, 2024 Accessed: Oct. 29, 2025. [Online]. Available: https://patentscope.wipo.int/search/en/WO2024173741

[44] Y. Qiao *et al.*, "Experimental study of thermal energy storage-integrated vapor compression system for load shifting in space cooling and heating," presented at the 15th IEA Heat Pump Conference, Vienna, May 2026.

[45] AHRI Standard 210/240, "Standard for Performance Rating of Unitary Air-Conditioning and Air-Source Heat Pump," 2017.

[46] S. Wilcox and W. Marion, "Users Manual for TMY3 Data Sets (Revised)," National Renewable Energy Lab. (NREL), Golden, CO (United States), NREL/TP-581-43156, May 2008. doi: 10.2172/928611.

[47] V. Ayyagari, A. Shooshtari, and M. Ohadi, "Glauber's Salt Composites for HVAC Applications: A Study on the Use of the T-History Method with a Modified Data Evaluation Methodology," *Materials*, vol. 18, no. 2998, doi: https://doi.org/10.3390/ma18132998.

[48] A. Othman, V. Aute, and J. Tancabel, "Recharge Demand Mitigation for Latent Heat Thermal Energy Storage at Off-Peak Hours," *Int. High Perform. Build. Conf.*, Jan. 2024, [Online]. Available: https://docs.lib.purdue.edu/ihpbc/453